J Solid State Electrochem (2004) 8: 935–940
DOI 10.1007/s10008-004-0511-3

ORIGINAL PAPER

Kyung-Hwan Na · Su-Il Pyun

Analysis of electrochemical impedance spectra of anodised pure aluminium foil with various etch tunnel length distributions used for electrolytic capacitors

Received: 14 November 2003 / Accepted: 7 January 2004 / Published online: 23 March 2004

Abstract The present work analyses the electrochemical impedance spectra of anodized pure Al foil with various etch tunnel length distributions, used for electrolytic capacitors. The lengths of the etch tunnels formed on the Al foil specimen were more widely distributed with increasing etching time. The etch tunnel length distributions were quantitatively measured by scanning electron microscopy. All the measured impedance spectra hardly exhibited the ideal capacitive behaviour in the high-frequency region and they deviated more significantly from the ideal capacitive behaviour with increasing etching time. For the numerical calculation of the total impedance of the electrode, the transmission line model was modified to reflect the etch tunnel length distribution, which represents the respective contributions of etch tunnels with different lengths to the total impedance. The total impedance was calculated by the integration of the impedance of one etch tunnel with respect to the etch tunnel length by taking the value of the etch tunnel length distribution determined experimentally. From the coincidence of the impedance spectra calculated numerically with those spectra measured experimentally, it is concluded that the deviation of the impedance spectra from the ideal capacitive behaviour in the high-frequency region originates from the characteristic frequency dispersion that depends upon the etch tunnel length distribution.

Keywords Aluminium · Etch tunnel · Electrochemical impedance spectroscopy · Transmission line model

K.-H. Na · S.-I. Pyun (✉)
Department of Materials Science and Engineering,
Korea Advanced Institute of Science and Technology,
373-1 Guseong-dong, Yuseong-gu, 305-701 Daejeon,
Republic of Korea
E-mail: sipyun@webmail.kaist.ac.kr
Tel.: +82-42-8693319
Fax: +82-42-8693310

Introduction

Electrochemical etching of Al foil is an important industrial process used for increasing the capacitance of Al electrolytic capacitors, since this process can be effectively utilised to increase the surface area of the Al foil by the formation of etch tunnels. Among various etching methods, DC etching has been employed to grow etch tunnels in the direction perpendicular to the foil surface for high-voltage applications [1, 2].

A considerable number of studies have been made on the characterisation of the morphologies of etch tunnels by using scanning electron microscopy (SEM) [3, 4, 5, 6, 7, 8]. It has been reported [5, 7, 8] that etch tunnels formed on the Al electrode were variously distributed in length, but those tunnels maintain approximately constant widths. Especially, Beck et al. [5] developed a mathematical model for determining the length distribution of etch tunnels by assuming that the death fraction of etch tunnels per unit length during the etch tunnel growth is constant.

The transmission line model, which was first introduced by de Levie [9, 10], has been widely used to interpret the impedance behaviour of porous electrodes. In recent years, especially the effects of pore size or length distribution have been investigated, based upon the transmission line model [11, 12, 13, 14, 15]. Similar to the case of porous electrodes, the ions in electrolytes should migrate through etch tunnels to be accumulated at the bottom of the tunnels, when the Al electrode is composed of etch tunnels. This strongly indicates that the transmission line model can be successfully applied to the analysis of the impedance behaviour of an electrode with etch tunnels. Considering that etch tunnels are widely distributed in length, it is readily expected that the impedance of an electrode with etch tunnels may be affected by the etch tunnel length distribution. Therefore, it is necessary to investigate the effect of the etch tunnel length distribution on the impedance behaviour of an electrode.

The present work was performed in order to analyse the electrochemical impedance spectra of an anodised Al electrode with various etch tunnel length distributions. For this purpose, the transmission line model was first modified by taking the etch tunnel length distribution into account. The total impedance was then calculated numerically from the equation for the transmission line model by using the value of the etch tunnel length distribution determined experimentally.

Experimental

The test specimen used in this work was high-purity (99.99%) 1-mm thick Al foil. The impurity concentration in the specimen used in this study is given in Table 1. For a high cubicity texture, all the specimens were annealed at 560 °C for 18 h.

Before electrochemical etching, pretreatment was performed on the specimen by immersion in aqueous 1 M NaOH solution at room temperature for 10 min to enhance uniformity in the lateral distribution of etch tunnels over the specimen surface. Galvanostatic etching was carried out in aqueous 1 M HCl solution at 70 °C at a constant current density of 100 mA cm^{-2} for various durations of time. The oxide film was formed on the specimen by anodising in aqueous 0.5 M $H_3BO_3 + 0.05$ M $Na_2B_4O_7$ solution. A current density of 0.5 mA cm^{-2} was applied until 50 V was reached, and the specimen was then held at 50 V for a further 30 min.

Electrochemical impedance measurement was carried out at room temperature by applying an AC amplitude of 5 mV on open-circuit potential over the frequency range 10^{-1} to 10^5 Hz. A 50/50 vol% mixture of glycerol and aqueous 0.5 M $H_3BO_3 + 0.05$ M $Na_2B_4O_7$ was used as electrolyte. Here, glycerol was added to the solution in order to lower the ionic conductivity, and thereby to clearly observe the impedance behaviour associated with ion migration through etch tunnels.

In all electrochemical experiments, a platinum gauze and a Ag/AgCl/4 M KCl electrode were used as the counter and reference electrodes, respectively.

The morphology of the etch tunnels was observed using the oxide replication technique [3]. Metallic Al was first dissolved from the anodised foil by immersion in bromine/methanol solution. After that, the remained oxide replica was observed by using SEM. The etch tunnel length distribution at each etching time was finally determined from six SEM micrographs of the oxide replica of the etched specimen at magnifications of 500 to 1000.

Results and discussion

Determination of the etch tunnel length distribution

Figure 1 presents the XRD pattern of the Al foil specimen obtained by the θ-2θ scanning method for examining the preferred orientation. In this figure, it was shown that the diffraction peak from (200) plane was the most dominant one and hence the surface of the specimen mainly consisted of (100) planes.

Table 1 Impurity concentration in the pure Al foil specimen (in wt ppm)

Fe	Mg	Ce	Cu	Ta	La	Ba	Ca	Na	K	Zn
1.9	1.4	1.4	1.2	1.0	0.91	0.57	0.4	0.3	0.16	0.15

A typical SEM micrograph of the oxide replica of the Al foil specimen etched in 1 M HCl at 70 °C at an anodic current density of 100 mA cm^{-2} for 15 s is shown in Fig. 2. It was observed that most of etch tunnels grew in the direction perpendicular to the surface of the specimen. Considering that etch tunnels grow preferentially along [100] direction by DC etching [1, 6], this is another indication that the Al foil specimen used in this work has (100) preferred orientation. Also, it was found that the lengths of the etch tunnels were widely distributed, whereas the widths of the etch tunnels were about 1 μm regardless of the etching time. This value of the etch tunnel width coincides quite well with the value reported in the literature [7, 8].

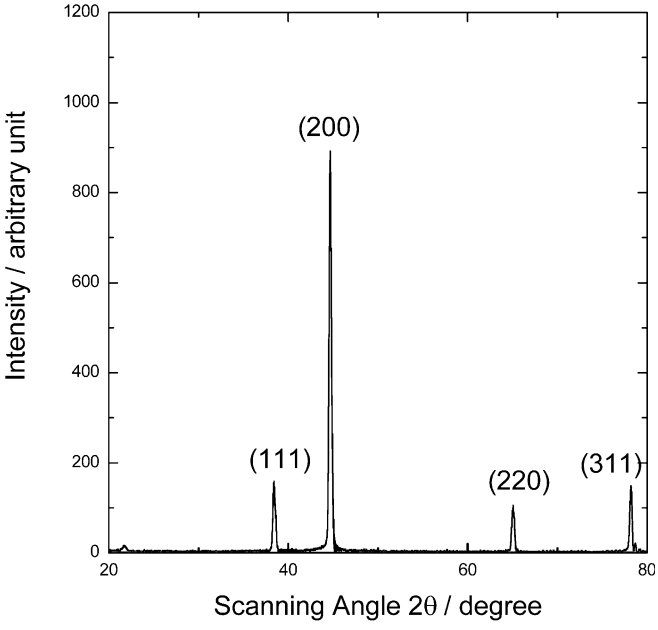

Fig. 1 XRD pattern of an Al foil specimen obtained by the θ-2θ scanning method for examining the preferred orientation

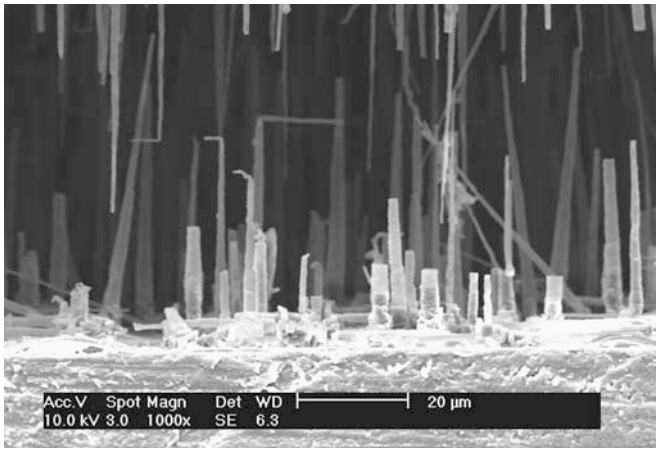

Fig. 2 SEM micrograph of the oxide replica of an Al foil specimen etched in 1 M HCl at 70 °C for 15 s at a constant anodic current density of 100 mA cm^{-2}

In the present work, the etch tunnel length distribution was estimated experimentally according to the mathematical model suggested by Beck et al. [5]. In their model, it is assumed that the death fraction of etch tunnels per unit length during the etch tunnel growth is constant. The etch tunnel length distribution function, $F(l,t)$ (μm^{-1}), can be given by:

$$F(l,t) = \delta(l-ut)\exp(-K_D l) + K_D \exp(-K_D l)[2 + K_D(ut-l)]; \quad l \leqslant ut \quad (1)$$

and:

$$F(l,t) = 0; \quad l > ut \quad (2)$$

where $\delta(l-ut)$ is the Dirac delta function, l is the length of an etch tunnel under consideration (μm), t is the etching time (s), u is the etch tunnel growth rate ($\mu m\ s^{-1}$) and K_D is the death fraction of etch tunnels per unit length during the etch tunnel growth (μm^{-1}). $\delta(l-ut)$ has a value of ∞ at $l=ut$, and zero elsewhere. In Eq. 1, the first term on the right-hand side represents the contribution of etch tunnels generated at $t=0$ to $F(l,t)$ and the second term is that of etch tunnels generated after $t=0$ to $F(l,t)$.

If we neglect the contribution of the initially generated etch tunnels to $F(l,t)$ and dimensionalise $F(l,t)$ for unit area by multiplying the number of etch tunnels per unit area, N (μm^{-2}), the etch tunnel number density, $NF(l,t)$ (μm^{-3}), can be obtained as follows:

$$NF(l,t) \approx N\{K_D \exp(-K_D l)[2 + K_D(ut-l)]\} \quad (3)$$

In order to determine the etch tunnel growth rate, u, the length of the longest etch tunnel was plotted against the etching time, as shown in Fig. 3. The value of u was then measured as 0.83 $\mu m\ s^{-1}$ from the slope in the plot of the longest etch tunnel length versus the etching time.

Figure 4 shows the plots of the etch tunnel number density, $NF(l,t)$, of the Al electrode against the distance from surface at various etching times, obtained from SEM micrographs such as Fig. 2. Since etch tunnels counted at a given distance from surface have lengths equivalent to the distance from surface, the distance from surface directly means the etch tunnel length. It was found that the etch tunnel number density decreased with increasing etch tunnel length as a whole. It is also noted that the maximum peak due to the initially generated etch tunnels was absent in Fig. 4. This implies that the assumption that the contribution of the initially generated etch tunnels to $F(l,t)$ can be ignored is reasonable.

The etch tunnel number density, $NF(l,t)$, in Fig. 4 was fitted to Eq. 3 at two arbitrary points to obtain the values of K_D and N. The values of K_D and N were determined to be in the range of 1.2×10^{-2} to 4.6×10^{-2} μm^{-1} and 0.27 to 0.83 μm^{-2}, respectively. Particularly, the values of K_D ranged in the same order of magnitude as those values reported previously [5]. Figure 5 presents the etch tunnel length distribution functions, $F(l)$, of the electrodes etched for various times. It can be seen from Fig. 5 that the lengths of the etch tunnels were more widely distributed with increasing etching time.

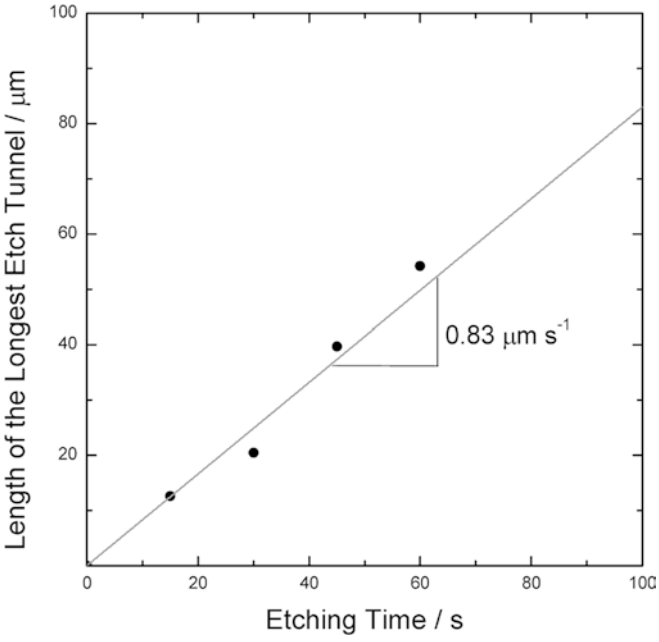

Fig. 3 Plot of the length of the longest etch tunnel against the etching time

Analysis of the impedance of the electrode based upon the modified transmission line model

In this work, the transmission line model [9, 10] was employed for analysing the impedance behaviour of the Al electrode composed of etch tunnels. Keeping in mind that the growth direction of the etch tunnels was perpendicular to the surface of the electrode as shown in Fig. 2, it is reasonable to assume that the equipotential line within the etch tunnel, to which the ions in electrolyte can penetrate, is perpendicular to the etch tunnel axis. In addition, if we assume that the shape of the etch tunnel is cylindrical and only a double-layer capacitance of the electrode/electrolyte interface contributes to the interfacial impedance, the impedance of one etch tunnel, Z_0 (Ω) [9, 10, 15], according to the transmission line model is given by:

$$Z_0 = (1-j)\left(\frac{R_{sol}}{2\omega C_{dl}}\right)^{1/2} \coth\left[(1+j)\left(\frac{\omega R_{sol} C_{dl}}{2}\right)^{1/2} l\right] \quad (4)$$

where R_{sol} is the solution resistance inside an etch tunnel per unit etch tunnel length ($\Omega\ \mu m^{-1}$), C_{dl} is the double-layer capacitance per unit etch tunnel length ($F\ \mu m^{-1}$) and ω is the angular frequency ($rad\ s^{-1}$).

If N etch tunnels with the same width and length per unit area are located in parallel, the total impedance of the electrode, Z_{tot}($\Omega\ \mu m^2$), is just given by:

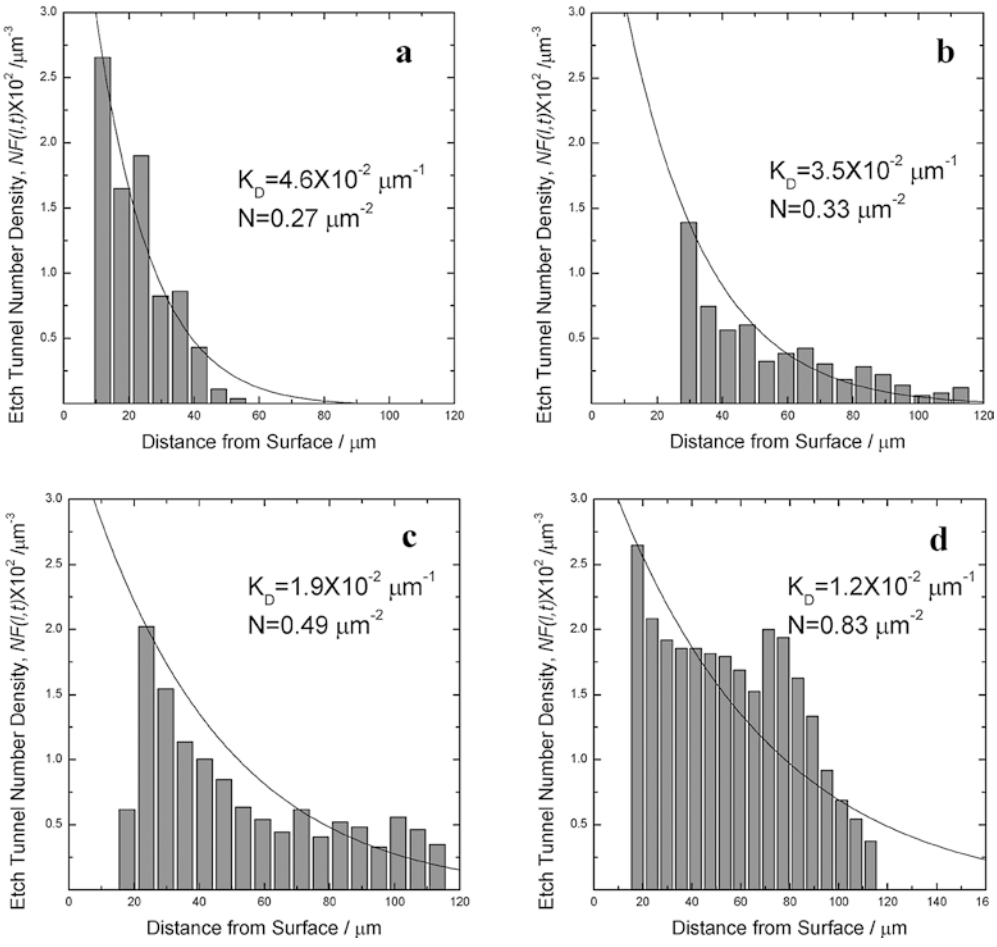

Fig. 4a–d Plots of the etch tunnel number density, $NF(l,t)$, versus the distance from surface obtained experimentally. *Lines* represent the etch tunnel number density fitted theoretically. The Al electrode was etched for various times of (**a**) 60 s, (**b**) 90 s, (**c**) 120 s and (**d**) 150 s

$$Z_{\text{tot}} = \frac{Z_0}{N} \tag{5}$$

It has been generally known that the impedance spectrum calculated from Eq. 5 can be divided into two regions in the Nyquist plot: (1) a straight line inclined at 45° to the real axis in the high-frequency region, and (2) a vertical line in the low-frequency region [14, 15].

As the angular frequency, ω, decreases during the electrochemical impedance measurement, the equipotential line moves from the orifice of the etch tunnel to the bottom of the etch tunnel. In this case, the penetration depth, l_p (μm) [16], is given by:

$$l_p = \frac{1}{(\omega R_{\text{sol}} C_{\text{dl}})^{1/2}} \tag{6}$$

If l_p is smaller than the etch tunnel length l at high frequencies, the impedance spectrum exhibits a Warburg straight line inclined at 45° to the real axis, associated with the semi-infinite ion migration through the etch tunnel [14, 15]. In contrast, if l_p exceeds l at sufficiently low frequencies, a vertical line due to the accumulation of ions at the bottom of the etch tunnel appears in the

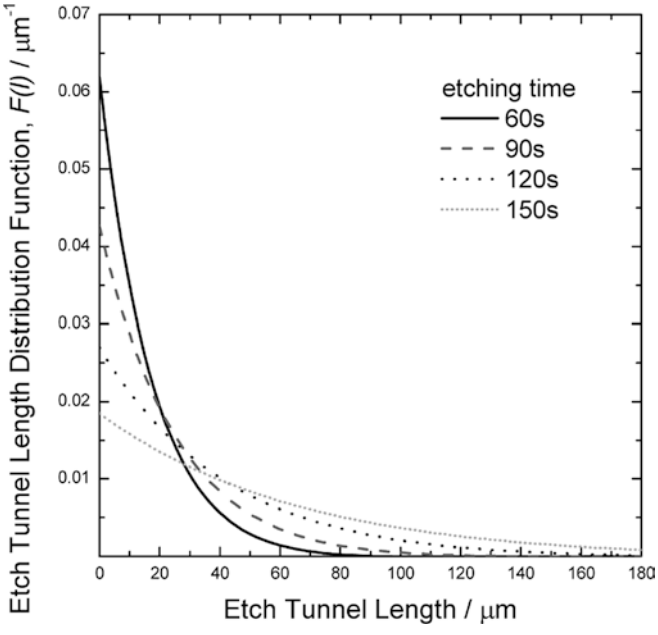

Fig. 5 Etch tunnel length distribution functions, $F(l)$, determined from Fig. 4 at various etching times

impedance spectrum. The characteristic frequency, f_c (Hz), between the two regions is defined as the frequency at which the ions in the electrolyte reach the bottom of the etch tunnel and is then expressed as follows [17, 18]:

$$f_c = \frac{\omega_c}{2\pi} = \frac{1}{2\pi R_{sol} C_{dl}} \frac{1}{l^2} \tag{7}$$

where ω_c is the characteristic angular frequency (rad s^{-1}). As a consequence, f_c represents the measure of how fast the whole surface of the etch tunnel can be electrochemically accessible. This is not unlike the inverse of the break-through time in hydrogen permeation current transients [19]. The characteristic frequency, f_c, approximates to the frequency which corresponds to the inflexion point of the impedance spectrum in the Nyquist plot. That means, in the case of etch tunnels with the same length, that f_c appears sharply at a unique point of the impedance in either the Nyquist plot or the Bode plot.

Figure 6 depicts the Nyquist plot of the impedance spectra (symbols) measured experimentally from the anodized Al foil with various etch tunnel length distributions. All the measured impedance spectra in the high-frequency region deviated in shape from the ideal capacitive behaviour. Furthermore, they never even exhibited the Warburg behaviour which was expected from an electrode composed of etch tunnels with the same length: the slope in the Nyquist plot at a given frequency never showed a constant value of 45° but it increased monotonically from a value higher than 45° to approximately 90° with decreasing frequency. In addition, the value of the instantaneous slope in the Nyquist plot increased more slowly to 90° with increasing etching time, implying that the impedance spectra deviated more significantly from the ideal capacitive behaviour with increasing etching time.

In order to clarify the origin of such a non-ideal behaviour of the impedance spectra, the total impedance of the electrode was calculated numerically, based upon the modified transmission line model by taking into account the etch tunnel length distribution, $F(l)$.

Provided that etch tunnels with different lengths are located in parallel, the total impedance of the electrode, Z_{tot} (Ω μm^2), is expressed in an analytical form as follows:

$$\frac{1}{Z_{tot}} = \int_0^{ut} \frac{N}{Z_0} F(l)\, dl \tag{8}$$

where $NF(l)dl$ represents the number of etch tunnels with length between l and $l + dl$ per unit area. In Eq. 8, the etch tunnel length distribution function $F(l)$ represents the respective contributions of etch tunnels with different lengths l to the total impedance. Considering that the characteristic frequency f_c is inversely proportional to the square of the etch tunnel length l according to Eq. 7, f_c is widely distributed over the whole range of the total impedance Z_{tot}.

The total impedances of the electrodes with various etch tunnel length distributions were calculated numer-

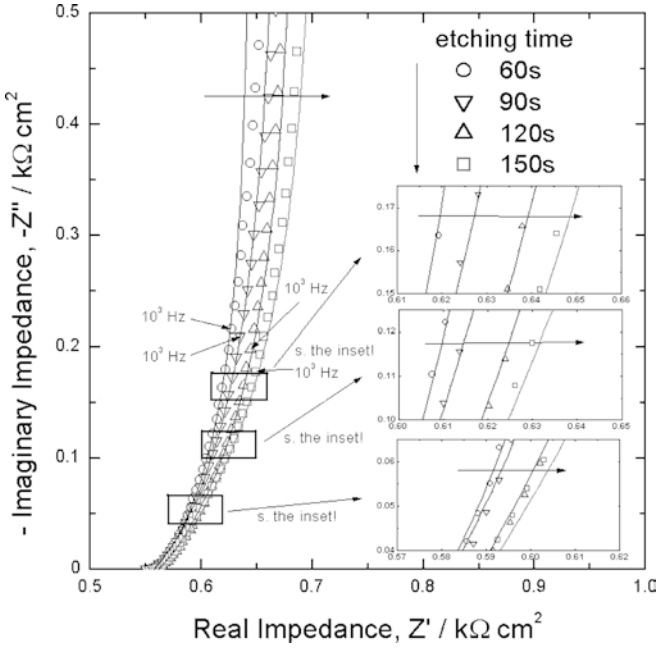

Fig. 6 Impedance spectra in Nyquist presentation of the anodised Al foil specimen in a solution of 50 vol% (0.5 M H_3BO_3 + 0.05 M $Na_2B_4O_7$) + 50 vol% glycerol at various etching times. *Lines* represent the impedance spectra calculated numerically, based upon the modified transmission line model in consideration of the etch tunnel length distribution given in Fig. 5

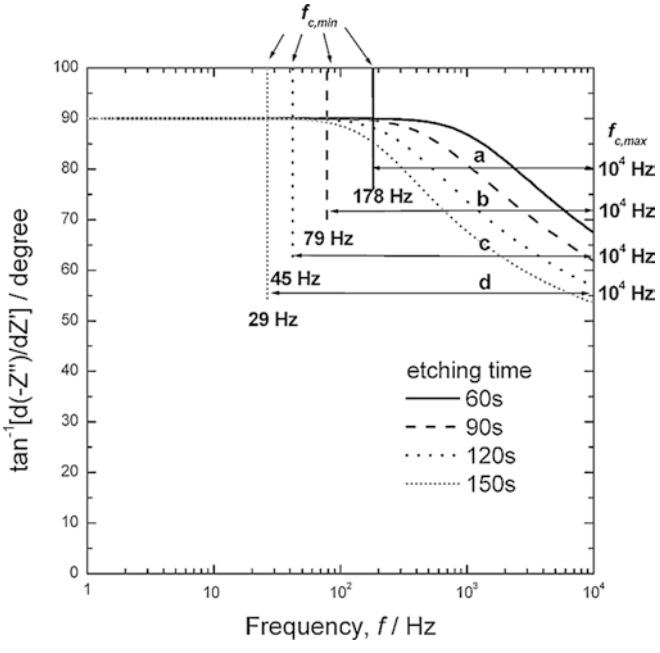

Fig. 7 Plots of $\tan^{-1}[d(-Z'')/d\ Z']$ versus frequency (Bode plot) calculated numerically at various etching times of (**a**) 60 s, (**b**) 90 s, (**c**) 120 s and (**d**) 150 s, based upon the modified transmission line model in consideration of the etch tunnel length distribution given in Fig. 5. *Arrow* represents the characteristic frequency dispersion

ically from Eq. 8 by taking N and $F(l)$ as the values given in Fig. 4 and Fig. 5, respectively, and the resulting impedance spectra are presented in Fig. 6 (full lines) along with those impedance spectra measured experimentally (symbols). The impedance spectra calculated numerically were in good agreement in both shape and value with the impedance spectra obtained experimentally. Therefore, it can be said that the deviation of the impedance spectra from the ideal capacitive behaviour in the high-frequency region is mainly attributable to the characteristic frequency dispersion which is caused by the etch tunnel length distribution.

Figure 7 demonstrates the plots of $\tan^{-1}[\mathrm{d}(-Z'')/\mathrm{d}\,Z']$ (phase angle) versus frequency at various etching times, which were reproduced from the numerically calculated impedance spectra given in Fig. 6. It is clearly shown that the value of the phase angle increased more slowly to 90° with increasing etching time, as indicated in Fig. 6. In Fig. 7, the maximum characteristic frequency, $f_{c,max}$, arises from the shortest etch tunnel. By contrast, the minimum characteristic frequency, $f_{c,min}$, results from the longest etch tunnel. As a consequence, the characteristic frequency dispersion from $f_{c,max}$ to $f_{c,min}$, designated as an arrow in Fig. 7, was more widespread with increasing etching time.

In conclusion, the impedance spectra deviated more significantly from the ideal capacitive behaviour with increasing etching time. This can be accounted for in terms of the characteristic frequency dispersion: the wider the etch tunnel length distribution is, the more markedly appears the characteristic frequency dispersion with increasing etching time.

Acknowledgements The receipt of a research grant (no. R01-2000-000-00240-0) from Korea Science & Engineering Foundation is gratefully acknowledged. Additionally, this work was partly supported by the Brain Korea 21 project. The authors are indebted to Mr. J.-W. Lee in the corrosion and interfacial electrochemistry research laboratory at KAIST for his helpful discussions.

References

1. Lin W, Tu GC, Lin CF, Peng YM (1997) Corros Sci 39:1531
2. Goad DGW, Uchi H (2000) J Appl Electrochem 30:285
3. Dunn CG, Bolon RB (1969) J Electrochem Soc 116:1050
4. Dunn CG, Bolon RB, Alwan AS, Stirling AW (1971) J Electrochem Soc 118:381
5. Beck TR, Uchi H, Hebert KR (1989) J Appl Electrochem 19:69
6. Wiersma BJ, Hebert KR (1991) J Electrochem Soc 138:48
7. Osawa N, Fukuoka K (2000) Corros Sci 42:585
8. Tak YS, Sinha N, Hebert KR (2000) J Electrochem Soc 147:4103
9. de Levie R (1963) Electrochim Acta 8:751
10. de Levie R (1967) Electronical response of porous and rough electrodes, In Delahay P (ed) Advances in electrochemistry and electrochemical engineering, vol VI. Wiley, New York, pp 329–397
11. Eloot K, Debuyck F, Moors M, van Peteghem AP (1995) J Appl Electrochem 25:326
12. Eloot K, Debuyck F, Moors M, van Peteghem AP (1995) J Appl Electrochem 25:334
13. Nguyen PH, Paasch G (1999) J Electroanal Chem 460:63
14. Song HK, Jung YH, Lee KH, Dao LeH (1999) Electrochim Acta 44:3513
15. Lee GJ, Pyun SI, Kim CH (2004) J Solid State Electrochem 8:110
16. Kim CH, Pyun SI, Shin HC (2002) J Electrochem Soc 149:A93
17. Grzeszczuk M, Olszak GZ (1993) J Electroanal Chem 359:161
18. Skinner NG, Hall EAH (1994) Synth Met 63:133
19. Boes N, Züchner H (1976) J Less-Common Met 49:223